The strength of the meridional overturning circulation of the stratosphere

Marianna Linz*

Massachusetts Institute of Technology–Woods Hole Oceanographic Institution Joint Program in Physical Oceanography, Massachusetts Institute of Technology, Cambridge, MA, USA

R. Alan Plumb

Department of Earth, Atmospheric and Planetary Sciences, Massachusetts Institute of Technology, Cambridge, MA, USA

Edwin P. Gerber

Courant Institute of Mathematical Sciences, New York University, New York, NY, USA

Florian J. Haenel

Karlsruhe Institute of Technology, Institute of Meteorology and Climate Research, Karlsruhe, Germany

Gabriele Stiller

Karlsruhe Institute of Technology, Institute of Meteorology and Climate Research, Karlsruhe, Germany

Douglas E. Kinnison

Atmospheric Chemistry Observations and Modeling Laboratory, National Center for Atmospheric Research, Boulder, CO, USA

Alison Ming

Department of Applied Mathematics and Theoretical Physics, University of Cambridge, Cambridge, UK

Jessica L. Neu

Jet Propulsion Laboratory, California Institute of Technology, Pasadena, California, USA

**Corresponding author address:* Marianna Linz, 54-1615, Massachusetts Institute of Technology, Cambridge, MA 02139

E-mail: mlinz@mit.edu

ABSTRACT

The Brewer–Dobson circulation, the meridional overturning of mass in the stratosphere, is important for the distribution of gases in the stratosphere, such as ozone and water vapor, which impact surface climate Previously, no observations-based estimate of its global strength existed. We present two such calculations of the mean strength of the meridional overturning of the stratosphere, quantified by the global diabatic circulation, between 2007–2011 from satellite data and compare these to three reanalyses and a state-of-the-art model. Using measurements of sulfur hexafluoride (SF_6) and nitrous oxide, we calculate the global mean diabatic overturning mass flux at all isentropic levels within the stratosphere. In the lower stratosphere, these two estimates agree, and at 460 K (about 20 km or 60 hPa in tropics), the global circulation strength is $7.3 \pm 0.3 \times 10^9$ kg/s. In that region, the reanalyses broadly agree. Higher in the atmosphere, only the SF_6 data-based estimate is available, and it diverges from the reanalyses and model. Interpretation of the SF_6 data-based estimate is limited by the mesospheric sink of SF_6; however, the reanalyses also differ substantially from each other, implying 100% uncertainty in the mean meridional overturning circulation strength at upper levels.

Previous calculations of the strength of the stratospheric circulation from data have relied on indirect measures. Observational estimates of the strength of the overturning have been limited to qualitative descriptions based on tracer distributions (e.g. Stiller et al. 2012, Engel et al. 2009, Mahieu et al. 2014, Haenel et al. 2015) or quantitative measures of very limited regions, such as the vertical velocity over a narrow range in the tropics (Mote et al. 1996, Schoeberl et al. 2008,Flury et al. 2013). Free-running climate models vary widely in stratospheric circulation metrics, including the tropical upwelling mass flux at 10 hPa and 70 hPa, though the multimodel mean is relatively close to some reanalysis products (Butchart et al. 2011). Reanalyses, meanwhile, differ substantially in their mean tropical upwelling velocity, with the magnitude of the mismatch depending on how it is computed (Abalos et al. 2015). Here we consider the diabatic circulation of the stratosphere; because the stratosphere is stratified, vertical motion moves air across potential temperature surfaces and thus must be associated with warming/cooling in the ascending/descending branches. Hence the net meridional overturning of mass is tightly linked to diabatic processes. We use potential temperature as our vertical coordinate and the meridional overturning becomes explicitly the diabatic circulation in this framework.

In a generalization of the work by Neu and Plumb (1999), Linz et al. (2016) presented a theory to calculate the strength of the diabatic stratospheric circulation through each isentropic surface above the tropical tropopause from the idealized tracer "age of air" (Waugh and Hall 2002), which is a measure of how long a parcel of air has spent in the stratosphere. The difference between the age of the air that is upwelling and downwelling through an isentropic surface is inversely proportional to the strength of the diabatic circulation through that surface, in steady-state and neglecting diabatic diffusion.

In this paper, we apply the age difference theory to calculate the mean magnitude and vertical structure of the global overturning circulation of the stratosphere based on observations of sulfur hexafluoride (SF_6) and nitrous oxide (N_2O). We demonstrate the validity of the theory and explore limitations of the tracer data with a coupled chemistry-climate model. We calculate the magnitude and vertical structure of the global overturning directly from the diabatic vertical velocity from three reanalyses to compare with the data and model results. Information on the data products, model, and reanalyses is given in Table 1.

1. Age of air observations and model

A trace gas that is linearly increasing in time in the troposphere and has no stratospheric sinks can be converted to age following the theory presented in Waugh and Hall (2002). Carbon dioxide (CO_2) and SF_6 are both approximately linearly increasing in the troposphere and have minimal sinks in the stratosphere. We use age derived from sulfur hexafluoride (SF_6) measurements (henceforth SF_6-age) from the Michelson Interferometer for Passive Atmospheric Sounding (MIPAS) on Envisat (Haenel et al. 2015). We interpolate SF_6-age onto isentropic surfaces using simultaneously retrieved pressure and temperature from MIPAS (von Clarmann et al. 2003, 2009). The resulting SF_6-age on the 500 K surface is shown in Figure 1a. Age is young in the tropics, older in the extratropics, and oldest at the winter poles, consistent with the pattern of upwelling in the tropics and the majority of downwelling in the winter polar region. The SF_6-age at high latitudes in wintertime is older than observations of age based on CO_2 measurements (Plumb et al. 2002). SF_6 is not conserved in the mesosphere, and its sink will result in a high bias in SF_6-age in areas with mesospheric influence (Hall and Waugh 1998), such as the poles and the upper stratosphere.

To explore the limitations of using SF_6-age, we compare SF_6-age to ideal age of air in a coupled chemistry-climate model, the Community Earth System Model 1 Whole Atmosphere Community Climate Model (WACCM). This is a fully coupled state-of-the-art interactive chemistry climate model (Marsh et al. 2013; Garcia et al. 2017). WACCM includes the physical parameterizations and finite-volume dynamical core (Lin 2004) from the Community Atmosphere Model, version 4 (Neale et al. 2013). The model domain extends from the Earth's surface to the lower thermosphere (140 km). The WACCM simulations examined are based on the Chemistry Climate Model Initiative REF-C1 scenario (Morgenstern et al. 2017). WACCM models only one of the two sinks of SF_6 in the mesosphere; photolysis at Lyman-alpha wavelengths is included, but associative electron attachment, which has recently been shown to be the dominant loss mechanism for SF_6 below 105 km (Totterdill et al. 2015; Kovács et al. 2017), is not. The impact of the mesospheric sink of SF_6 on the stratospheric SF_6 will be determined by the strength of the dynamical coupling between the stratosphere and the mesosphere. We calculate SF_6-age following the methods of Stiller et al. (2012) to compare with the MIPAS SF_6-age, for details see the Methods section. Although WACCM is missing the dominant SF_6 loss mechanism, the difference between SF_6-age and ideal age will qualitatively illustrate the type and location of any bias introduced by using SF_6 as an age tracer.

Age on the 500 K surface between 2002 and 2012 is shown for WACCM SF_6-age in Figure 1c, and for WACCM ideal age of air in Figure 1d. The close agreement between the ideal age and SF_6-age on the 500 K surface suggests that SF_6-age is a good proxy for ideal age. The temporal correlation at each latitude on the 500 K surface is high ($r = 0.93$), and only at the poles is the SF_6-age older than the ideal age by up to half a year. Where there is more mesospheric influence, the correlation is weaker and is no longer one-to-one: higher in the stratosphere and at the highest latitudes ($r = 0.52$ and age has only 35% of the magnitude of variations of SF_6-age at 1200 K at 85° N). Since WACCM is missing the dominant sink of SF_6, the differences shown here represent a lower bound on the bias induced by using SF_6-age as a proxy for ideal age.

To corroborate the circulation strength calculations from SF_6-age, other age tracers are desirable. CO_2, is currently not retrieved from satellites with enough accuracy and spatial coverage to calculate age of air differences (Carlotti et al. 2016). Instead, we determine age from N_2O, which demonstrates a compact relationship with age, like other long-lived stratospheric tracers (Plumb and Ko 1992). We use the relationship between age of air and N_2O calculated empirically by Andrews et al. (2001), assuming that this compact relationship has not changed substantially in the interim while accounting for the linear growth in tropospheric N_2O. Following the procedure outlined in the Methods, we calculate age of air from the Global OZone Chemistry And Related trace gas Data records for the Stratosphere (GOZCARDS) N_2O data for 2004–2013 (Froidevaux et al. 2013). Because of the range of tracer values over which the empirical relationship holds, global coverage exists for a small range in potential temperature (about 450 K–500 K).

The age on the 500 K surface calculated from the empirical relationship of age with N_2O is shown in Figure 1b. The Southern Hemisphere winter polar coverage is poor on this level because values of N_2O are below 50 ppbv, the lower limit of the empirical fit. Age from the N_2O data is generally younger than MIPAS SF_6-age, though somewhat older than ages from WACCM. The temporal correlation of MIPAS SF_6-age and N_2O-age at every latitude on the 500 K surface is around $r = 0.5$, except in the Northern Hemisphere midlatitudes, where the correlation is not significant.

2. Age difference and the diabatic circulation

Linz et al. (2016) showed that, in steady state, the diabatic circulation ($\mathcal{M}$) through an isentropic surface wholly within the stratosphere can be calculated as the ratio of the mass above the surface (M) to the difference in the mass-flux-weighted age of downwelling and upwelling air on the surface ($\Delta\Gamma$, or age difference).

$$\mathcal{M} = M/\Delta\Gamma. \tag{1}$$

$\mathcal{M}$ is the total mass flux that is upwelling (or downwelling, as in steady-state these must be equal) through the isentropic surface. Intuitively this reflects the idea of a residence time; the age difference is how long the air spent above the surface, and it is equal to the ratio of the mass above the surface to the mass flux passing through that surface.

The real world is not in steady-state, and so some amount of averaging is necessary for this theory to apply. The MIPAS data has five years of continuous data, and so the longest average possible for this study is five years. To test the validity of applying this steady-state theory to five-year averages of age difference, we have calculated the 2007–2011 averages of ideal age difference and the ratio of the total mass above each isentrope to the mass flux through that isentrope from WACCM output. These are shown in the blue lines (solid and dotted respectively) in Figure 2. The total overturning strength is calculated from the potential temperature tendency, $\dot{\theta}$, which is the total all sky radiative heating rate interpolated onto isentropic surfaces. The upwelling and downwelling regions are defined based on where $\dot{\theta}$ is instantaneously positive or negative, and the mass fluxes through these regions are averaged to obtain the total overturning mass flux, $\mathcal{M}$. If the age difference theory held exactly, the two blue lines in Figure 2 would be identical. In the upper stratosphere, these two calculations agree closely; in the lower stratosphere, the ratio of the mass to the mass flux is greater than the ideal age $\Delta\Gamma$. This behavior is consistent with the neglect of diabatic diffusion, which is greater in the lower stratosphere (Sparling et al. 1997). Using area weighting of ideal age, since mass-flux weighting is not possible with data, results in about a 10% low bias of $\Delta\Gamma$ compared to the mass-flux weighting shown here.

We calculate the five year average (2007–2011) of the difference in area-weighted age of air in the regions poleward and equatorward of 35° from the SF_6-age from both MIPAS and WACCM, and from the N_2O-age. The results of this are shown in Figure 2. The MIPAS SF_6-age $\Delta\Gamma$ is notably different from the other estimates except around 450 K. At 400 K, it is much smaller, in part because of young polar air at that level (not shown). Starting around 500 K, MIPAS SF_6 $\Delta\Gamma$ is much greater than the model $\Delta\Gamma$ using either ideal age or SF_6-age. Age difference for N_2O is calculated only where there is data available over the entire surface at almost all times, 450–480 K. In this limited range, the age difference from N_2O-age is somewhat greater than the age difference from WACCM and agrees with the age difference calculated from MIPAS SF_6-age.

To gain insight into the role of the mesospheric sink, we compare the ideal age $\Delta\Gamma$ with SF_6-age $\Delta\Gamma$ in WACCM. The ideal age $\Delta\Gamma$ is the mass-flux-weighted age difference between upwelling and downwelling regions, and the SF_6-age $\Delta\Gamma$ from WACCM is calculated in the same way as the MIPAS SF_6-age $\Delta\Gamma$. Because of the area-weighting, we expect the SF_6-age $\Delta\Gamma$ to be 10% lower than the ideal age $\Delta\Gamma$. This is true from 450–550 K, but above that, the SF_6-age $\Delta\Gamma$ is either equal to or greater than the ideal age $\Delta\Gamma$, and at 1200 K SF_6-age $\Delta\Gamma$ is 50% greater. Since WACCM does not include the dominant sink of SF_6 for the mesosphere, the bias is certainly greater, and we cannot estimate an upper bound.

All three calculations of $\Delta\Gamma$ from the model as well as the $\Delta\Gamma$ from MIPAS SF_6-age show a peak somewhere in the middle stratosphere. This peak indicates a relative minimum of the diabatic velocity at that level, and so this provides evidence that there are indeed two branches of the circulation (Birner and Bönisch 2011) and is a straightforward diagnostic for the separation level.

3. Circulation from Reanalyses, Model, and Age

Figure 3 shows the total overturning circulation strength calculated using the ratio of the total mass above the isentrope to $\Delta\Gamma$ for the MIPAS SF_6-age and the N_2O-age. Total mass is determined from the simultaneously retrieved pressure in the former case and from pressure from the Modern Era Retrospective analysis for Research and Applications (MERRA, Rienecker et al. 2011) for N_2O. Also shown is the directly calculated overturning circulation strength from the three reanalysis products MERRA, Japanese 55-year Reanalysis (JRA 55, Kobayashi et al. 2015 and the ECMWF Reanalysis Interim (ERA-Interim, Dee et al. 2011), and from WACCM. The total overturning strength is calculated from the potential temperature tendency, $\dot{\theta}$, from the total diabatic heating rates from JRA 55 and ERA-Interim forecast products and from total temperature tendency provided by MERRA, and then following the same procedure as above for WACCM.

These six estimates of the strength of the circulation are quite different, as can be seen clearly by examining the circulation at individual levels. At the lowermost levels, the reanalyses tend to agree, while the MIPAS SF_6-age circulation estimate is much greater because of its very low $\Delta\Gamma$. In the range where we have estimates from both observational data sets, they agree closely and are flanked by the reanalyses, which vary more widely (within 35% of the mean of all estimates at that level). At 500 K and above, the MIPAS SF_6-age based circulation strength has the lowest value, and at 900 K and above, it is lower by a factor of three. The circulation strength from MIPAS SF_6-age $\Delta\Gamma$ is biased low consistent with the sink of SF_6 in the mesosphere (Kovács et al. 2017). The disagreement at 1200 K would require that the bias from using SF_6-age $\Delta\Gamma$ be nearly 300% for the model and reanalyses to be correct. In addition to the disagreement of MIPAS SF_6-age circulation strength with the model and reanalyses, there is significant disagreement between different reanalyses. MERRA has a distinct vertical structure, with weaker circulation in the lower stratosphere and stronger circulation in the mid stratosphere. JRA 55 and ERA Interim have a similar vertical structure; JRA 55 is stronger by around 3×10^9 kg s^{-1}, except above 800 K, where it decreases much more quickly than ERA-Interim so that they converge by 1200 K. The shading is the standard deviation of the annual averages that make up the five year average, and it shows the interannual variability, which is generally small.

4. Conclusions

In summary, we have calculated the strength of the overturning circulation of the stratosphere from observations, reanalyses, and a model. We find that at 460 K (about 60 hPa or 20 km in the tropics), the total overturning circulation of the stratosphere is 7.3 $\pm 0.3 \times 10^9$ kg/s based on two independent global satellite data products. Apart from that level, where the estimates are in relatively close agreement, substantial discrepancies exist.

The global SF_6 data have enabled this first quantitative calculation of the diabatic circulation in the middle and upper stratosphere. However, the interpretation of age from SF_6 is limited because we cannot quantify the impact of the mesospheric sink of SF_6, which we find to be important above 500 K. We estimate that this makes the age difference a minimum of 60% too high at 1200 K, which would imply a 35% low bias in the overturning strength at 1200 K, and we cannot estimate an upper bound on the bias. The reanalyses may correctly represent the true stratospheric circulation where they agree at the uppermost levels, although at those levels the data becomes more limited (e.g. Dee and Uppala 2009). Beneath 900 K, however, the reanalyses disagree with each other as well as with the circulation strength implied by the data; it is clear that the existing data are not sufficient to constrain estimates of the circulation.

Climate models predict an increase in the strength of the Brewer–Dobson circulation of about 2% per decade (Butchart et al. 2006, Hardiman et al. 2014), which will impact stratospheric ozone, including the ozone hole recovery, and stratosphere troposphere exchange (Butchart 2014). Much effort has recently gone towards calculating trends in the stratospheric circulation based on observations and reanalyses to see if such a trend can be detected (Engel et al. 2009, Seviour et al. 2012, Diallo et al. 2012, Abalos et al. 2015). However, the mean diabatic circulation strength is not known except at one level. At the upper levels, the circulation is uncertain to within 100%. We suggest cautious interpretation of trends that are much smaller than that uncertainty. More global age of air tracer data, in particular CO_2, is necessary to provide an independent estimate of age difference necessary to calculate the strength of the diabatic stratospheric circulation.

Methods

MIPAS SF_6 For more details on validation and methods, we refer the readers to the papers on this product (Stiller et al. 2008, 2012; Haenel et al. 2015). We note that the vertical resolution is 4 to 6 km at 20 km, 7 to 10 km at 30 km, and 12 to 18 km at 40 km altitude. Noise error on individual profiles is of the order 20%, but because of the many profiles, meaningful SF_6 has been obtained by using monthly and zonal mean averages in 10 degree bins.

N_2O Andrews et al. (2001) calculate an empirical fit between N_2O and age from an extensive record of NASA ER-2 aircraft flights and high-altitude balloons from 1992–1998. Age is based on CO_2, and for details of the conversion from CO_2 to age, see Andrews et al. (2001). The fit holds well for 50 ppbv $< N_2O <$ 300 ppbv and is given by the equation $\Gamma(N_2O) = 0.0581(313 - N_2O) - 0.000254(313 - N_2O)^2 + 4.41 \times 10^{-7}(313 - N_2O)^3$, where 313 ppbv was the average tropospheric mixing ratio for 1992–1998. Although different tracer-tracer relationships are expected in the tropics and the extratropics (e.g. Strahan et al. 2011, Plumb 2007), the limited tropical data used to calculate this relationship were not treated separately. In order to account for the increase in tropospheric N_2O, we calculate the trend from the data product provided by the EPA Climate Indicators (US Environmental Protection Agency 2016), a combination of station measurements from Cape Grim, Australia, Mauna Loa, Hawaii, the South Pole, and Barrow, Alaska. The slope is 0.806 ± 0.014 ppbv/yr. (One standard error on the slope is reported. Using only Mauna Loa, the tropical station, does not change the fit much, since N_2O is quite well mixed in the troposphere.) We linearly adjust the GOZCARDS N_2O data using this slope to account for the growth in tropospheric N_2O, although simply subtracting the mean difference in tropospheric N_2O between 2009 and 1995 yielded very similar results. Then we apply the empirical relationship between 2004 and 2012 to obtain age estimates. Age difference is calculated only on those levels for which there are very few gaps in age. Only 460 and 470 K have no gaps at all. This method relies on several potentially problematic assumptions: the compact relationship from the 1990s is assumed to be applicable over a decade later; the tropics are assumed be represented by this relationship well enough to obtain unbiased estimates of age difference; and linearly adjusting the data is assumed to sufficiently account for the changing tropospheric source.

WACCM SF_6 The method to calculate age from SF_6 in WACCM is as follows: The SF_6 on pressure levels is zonally averaged and then averaged in the same latitudinal bins that were used for MIPAS. That zonally averaged SF_6 is then converted to age following Stiller et al. (2012). The reference curve for SF_6 is the zonal mean value in the tropics at 100hPa just north of the equator (0.5° N) with a one year low-pass fourth order Butterworth filter applied to remove the weak seasonal cycle. Results are insensitive to the filtering provided the filter is sufficient to obtain a strictly increasing reference curve. We use the same method for correcting the age of air for the nonlinear tropospheric growth, with a Newtonian iteration (see Stiller et al. 2012 equation 3). The nonlinearity correction is insensitive to the choice of constant parameter used to describe the relationship of the width of the age spectrum with the age. Once the age is determined, it is interpolated to isentropic levels using zonal mean temperatures that have also been binned by latitude according to the MIPAS grid. No attempt is made either by Haenel et al. (2015) or in this work to adjust the age for the mesospheric sink.

Statistics for 460 K overturning To calculate the average overturning circulation strength where the two data estimates agree most closely (within 5% at 460 K), we average them. The error estimate is based on the variability in the total overturning circulation strength from WACCM calculated using SF_6-age to infer the circulation (M/SF_6-age $\Delta\Gamma$). We take the average of five annual averages chosen randomly from the annual averages from 1999–2014 100,000 times. The standard deviation of the 100,000 resulting mean circulation strength estimates (0.14×10^9 kg/s) is taken to be half of the error. We repeated this procedure using the true overturning circulation strength ($\mathcal{M}$) and found smaller variations in the standard deviation (0.09×10^9 kg/s). This error estimate assumes that WACCM represents the variability of the true circulation. The standard deviations of the five annual averages that were averaged for each data estimate were considerably smaller than these reported error bars. We therefore believe this is a conservative representation of the uncertainty in the diabatic circulation strength.

Acknowledgments. We thank Aditi Sheshadri and Susan Solomon for helpful discussions. Funding for ML was provided by the National Defense Science and Engineering Graduate fellowship. This work was supported in part by the National Science Foundation grant AGS-1547733 to MIT and and AGS-1546585 to NYU. FH was funded by the "CAWSES" priority programme of the German Research Foundation (DFG) under project STI 210/5-3 and by the German Federal Ministry of Education and Research (BMBF) within the "ROMIC" programme under project 01LG1221B. MIPAS data processing was co-funded by the German Federal Ministry of Economics and Technology (BMWi) within the "SEREMISA" project under contract number 50EE1547. AM acknowledges funding support from the European Research Council through the ACCI project (Grant 267760) lead by John Pyle. The National Center for Atmospheric Research (NCAR) is sponsored by the U.S. National Science Foundation. Any opinions, findings, and conclusions or recommendations expressed in the publication are those of the author(s) and do not necessarily reflect the views of the National Science Foundation. WACCM is a component of the Community Earth System Model (CESM), which is supported by the National Science Foundation (NSF) and the Office of Science of the U.S. Department of Energy. Computing resources were provided by NCAR's Climate Simulation Laboratory, sponsored by NSF and other agencies. This research was enabled by the computational and storage resources of NCAR's Computational and Information System Laboratory (CISL). A portion of the research was carried out at the Jet Propulsion Laboratory, California Institute of Technology, under a contract with the NASA Aeronautics and Space Administration. One of the datasets used for this study is from the Japanese 55-year Reanalysis (JRA-55) project carried out by the Japan Meteorological Agency (JMA). MERRA was developed by the Global Modeling and Assimilation Office and supported by the NASA Modeling, Analysis and Prediction Program. Source data files can be acquired from the Goddard Earth Science Data Information Services Center (GES DISC). ERA-Interim data provided courtesy ECMWF.

References

Abalos, M., B. Legras, F. Ploeger, and W. J. Randel, 2015: Evaluating the advective Brewer-Dobson circulation in three reanalyses for the period 1979–2012. *Journal of Geophysical Research, Atmospheres*, 1–21, doi:10.1002/2015JD023182, URL http://onlinelibrary.wiley.com/doi/10.1002/2015JD023182/full.

Andrews, A. E., and Coauthors, 2001: Mean ages of stratospheric air derived from in situ observations of CO, CH4, and N2O. *Journal of Geophysical Research*, **106**.

Birner, T., and H. Bönisch, 2011: Residual circulation trajectories and transit times into the extratropical lowermost stratosphere. *Atmospheric Chemistry and Physics*, **11 (2)**, 817–827, doi:10.5194/acp-11-817-2011, URL http://www.atmos-chem-phys.net/11/817/2011/.

Butchart, N., 2014: The Brewer-Dobson circulation. *Reviews of Geophysics*, doi:10.1002/2013RG000448.One.

Butchart, N., and Coauthors, 2006: Simulations of anthropogenic change in the strength of the Brewer–Dobson circulation. *Climate Dynamics*, **27 (7-8)**, 727–741, doi:10.1007/s00382-006-0162-4, URL http://link.springer.com/10.1007/s00382-006-0162-4.

Butchart, N., and Coauthors, 2011: Multimodel climate and variability of the stratosphere. *Journal of Geophysical Research*, **116 (D5)**, D05 102, doi:10.1029/2010JD014995, URL http://doi.wiley.com/10.1029/2010JD014995.

Carlotti, M., B. M. Dinelli, G. Innocenti, and L. Palchetti, 2016: A strategy for the measurement of CO_2 distribution in the stratosphere. *Atmospheric Measurement Techniques*, **9 (12)**, 5853–5867, doi:10.5194/amt-9-5853-2016, URL http://www.atmos-meas-tech.net/9/5853/2016/.

Dee, D. P., and S. Uppala, 2009: Variational bias correction of satellite radiance data in the era-interim reanalysis. *Quarterly Journal of the Royal Meteorological Society*, **135 (644)**, 1830–1841, doi:10.1002/qj.493, URL http://dx.doi.org/10.1002/qj.493.

Dee, D. P., and Coauthors, 2011: The ERA-Interim reanalysis: configuration and performance of the data assimilation system. *Quarterly Journal of the Royal Meteorological Society*, **137 (656)**, 553–597, doi:10.1002/qj.828, URL http://dx.doi.org/10.1002/qj.828.

Diallo, M., B. Legras, and a. Chédin, 2012: Age of stratospheric air in the ERA-Interim. *Atmospheric Chemistry and Physics*, **12 (24)**, 12 133–12 154, doi:10.5194/acp-12-12133-2012, URL http://www.atmos-chem-phys.net/12/12133/2012/.

Engel, A., and Coauthors, 2009: Age of stratospheric air unchanged within uncertainties over the past 30 years. *Nature Geoscience*, **2**, 28–31.

Flury, T., D. L. Wu, and W. G. Read, 2013: Variability in the speed of the Brewer–Dobson circulation as observed by Aura/MLS. *Atmospheric Chemistry and Physics*, **13 (9)**, 4563–4575, doi:10.5194/acp-13-4563-2013, URL http://www.atmos-chem-phys.net/13/4563/2013/.

Froidevaux, L., R. A. Fuller, A. Lambert, N. J. Livesey, P. F. Bernath, and K. A. Walker, 2013: GOZCARDS Source Data for Nitrous Oxide Monthly Zonal Averages on a Geodetic Latitude and Pressure Grid v1.01. NASA Goddard Earth Sciences Data and Information Services Center, URL https://doi.org/10.5067/MEASURES/GOZCARDS/DATA3012, doi: 10.5067/MEASURES/GOZCARDS/DATA3012.

Garcia, R. R., A. K. Smith, D. E. Kinnison, lvaro de la Cmara, and D. J. Murphy, 2017: Modification of the Gravity Wave Parameterization in the Whole Atmosphere Community Climate Model: Motivation and Results. *Journal of the Atmospheric Sciences*, **74 (1)**, 275–291, doi:10.1175/JAS-D-16-0104.1, URL http://dx.doi.org/10.1175/JAS-D-16-0104.1, http://dx.doi.org/10.1175/JAS-D-16-0104.1.

Haenel, F. J., and Coauthors, 2015: Reassessment of MIPAS age of air trends and variability. *Atmospheric Chemistry and Physics*, **15**, 13 161?13 176, doi:10.5194/acp-15-13161-2015, URL www.atmos-chem-phys.net/15/13161/2015/.

Hall, T. M., and D. W. Waugh, 1998: Influence of nonlocal chemistry on tracer distributions: Inferring the mean age of air from SF6. *Journal of Geophysical Research: Atmospheres*, **103 (D11)**, 13 327–13 336, doi:10.1029/98JD00170, URL http://dx.doi.org/10.1029/98JD00170.

Hardiman, S. C., N. Butchart, and N. Calvo, 2014: The morphology of the Brewer-Dobson circulation and its response to climate change in CMIP5 simulations. *Quarterly Journal of the Royal Meteorological Society*, **140 (683)**, 1958–1965, doi:10.1002/qj.2258, URL http://doi.wiley.com/10.1002/qj.2258.

Kobayashi, S., and Coauthors, 2015: The JRA-55 Reanalysis: General Specifications and Basic Characteristics. *Journal of the Meteorological Society of Japan. Ser. II*, **93 (1)**, 5–48, doi:10.2151/jmsj.2015-001.

Kovács, T., and Coauthors, 2017: Determination of the atmospheric lifetime and global warming potential of sulfur hexafluoride using a three-dimensional model. *Atmospheric Chemistry and Physics*, **17 (2)**, 883–898, doi:10.5194/acp-17-883-2017, URL http://www.atmos-chem-phys.net/17/883/2017/.

Lin, S.-J., 2004: A "Vertically Lagrangian" Finite-Volume Dynamical Core for Global Models. *Monthly Weather Review*, **132 (10)**, 2293–2307, doi:10.1175/1520-0493(2004)132⟨2293:AVLFDC⟩2.0.CO;2, URL http://dx.doi.org/10.1175/1520-0493(2004)132⟨2293:AVLFDC⟩2.0.CO;2, http://dx.doi.org/10.1175/1520-0493(2004)132⟨2293:AVLFDC⟩2.0.CO;2.

Linz, M., R. A. Plumb, E. P. Gerber, and A. Sheshadri, 2016: The relationship between age of air and the diabatic circulation of the stratosphere. *Journal of the Atmospheric Sciences*, **73 (11)**, 4507–4518, doi:10.1175/JAS-D-16-0125.1.

Mahieu, E., and Coauthors, 2014: Recent Northern Hemisphere stratospheric HCl increase due to atmospheric circulation changes. *Nature*, **515 (7525)**, 104–7, doi:10.1038/nature13857, URL http://www.ncbi.nlm.nih.gov/pubmed/25373680.

Marsh, D. R., M. J. Mills, D. E. Kinnison, J.-F. Lamarque, N. Calvo, and L. M. Polvani, 2013: Climate Change from 1850 to 2005 Simulated in CESM1(WACCM). *Journal of Climate*, **26 (19)**, 7372–7391, doi:10.1175/JCLI-D-12-00558.1, URL http://dx.doi.org/10.1175/JCLI-D-12-00558.1, http://dx.doi.org/10.1175/JCLI-D-12-00558.1.

Morgenstern, O., and Coauthors, 2017: Review of the global models used within phase 1 of the Chemistry–Climate Model Initiative (CCMI). *Geoscientific Model Development*, **10 (2)**, 639–671, doi:10.5194/gmd-10-639-2017, URL http://www.geosci-model-dev.net/10/639/2017/.

Mote, P. W., and Coauthors, 1996: An atmospheric tape recorder: The imprint of tropical tropopause temperatures on stratospheric water vapor. *Journal of Geophysical Research: Atmospheres*, **101 (D2)**, 3989–4006, doi:10.1029/95JD03422, URL http://dx.doi.org/10.1029/95JD03422.

Neale, R. B., J. Richter, S. Park, P. H. Lauritzen, S. J. Vavrus, P. J. Rasch, and M. Zhang, 2013: The Mean Climate of the Community Atmosphere Model (CAM4) in Forced SST and Fully Coupled Experiments. *Journal of Climate*, **26 (14)**, 5150–5168, doi:10.1175/JCLI-D-12-00236.1, URL http://dx.doi.org/10.1175/JCLI-D-12-00236.1, http://dx.doi.org/10.1175/JCLI-D-12-00236.1.

Neu, J. L., and R. A. Plumb, 1999: Age of air in a "leaky pipe" model of stratospheric transport. *J. Geophys. Res.*, **104 (D16)**, 19 243–19 255, doi:10.1029/1999JD900251.

Plumb, R. A., 2007: Tracer interrelationships in the stratosphere. *Reviews of Geophysics*, 1–33, doi:10.1029/2005RG000179.1.INTRODUCTION.

Plumb, R. A., and M. K. W. Ko, 1992: Interrelationships between mixing ratios of long-lived stratospheric constituents. *Journal of Geophysical Research: Atmospheres*, **97 (D9)**, 10 145–10 156, doi:10.1029/92JD00450, URL http://dx.doi.org/10.1029/92JD00450.

Plumb, R. A., and Coauthors, 2002: Global tracer modeling during SOLVE: High-latitude descent and mixing. *Journal of Geophysical Research: Atmospheres*, **107 (D5)**, doi:10.1029/2001JD001023, URL http://dx.doi.org/10.1029/2001JD001023, 8309.

Rienecker, M. M., and Coauthors, 2011: MERRA: NASA?s Modern-Era Retrospective Analysis for Research and Applications. *Journal of Climate*, **24 (14)**, 3624–3648, doi:10.1175/JCLI-D-11-00015.1, URL http://dx.doi.org/10.1175/JCLI-D-11-00015.1.

Schoeberl, M. R., A. R. Douglass, R. S. Stolarski, S. Pawson, S. E. Strahan, and W. Read, 2008: Comparison of lower stratospheric tropical mean vertical velocities. *Journal of Geophysical Research: Atmospheres*, **113 (D24)**, n/a–n/a, doi:10.1029/2008JD010221, URL http://dx.doi.org/10.1029/2008JD010221, d24109.

Seviour, W. J. M., N. Butchart, and S. C. Hardiman, 2012: The Brewer-Dobson circulation inferred from ERA-Interim. *Quarterly Journal of the Royal Meteorological Society*, **138 (665)**, 878–888, doi:10.1002/qj.966, URL http://doi.wiley.com/10.1002/qj.966.

Sparling, L. C., J. A. Kettleborough, P. H. Haynes, M. E. McIntyre, J. E. Rosenfield, M. R. Schoeberl, and P. A. Newman, 1997: Diabatic cross-isentropic dispersion in the lower stratosphere. *J. Geophys. Res.*, **102 (D22)**, 25 817–25 829, doi:10.1029/97JD01968.

Stiller, G. P., and Coauthors, 2008: Global distribution of mean age of stratospheric air from MIPAS SF_6 measurements. *Atmospheric Chemistry and Physics*, **8 (3)**, 677–695, doi:10.5194/acp-8-677-2008, URL http://www.atmos-chem-phys.net/8/677/2008/.

Stiller, G. P., and Coauthors, 2012: Observed temporal evolution of global mean age of stratospheric air for the 2002 to 2010 period. *Atmospheric Chemistry and Physics*, **12 (7)**, 3311–3331, doi:10.5194/acp-12-3311-2012, URL http://www.atmos-chem-phys.net/12/3311/2012/.

Strahan, S. E., and Coauthors, 2011: Using transport diagnostics to understand chemistry climate model ozone simulations. *Journal of Geophysical Research: Atmospheres*, **116 (D17)**, doi:10.1029/2010JD015360, URL http://dx.doi.org/10.1029/2010JD015360, d17302.

Totterdill, A., T. Kovcs, J. C. Gmez Martn, W. Feng, and J. M. C. Plane, 2015: Mesospheric Removal of Very Long-Lived Greenhouse Gases SF6 and CFC-115 by Metal Reactions, Lyman-α Photolysis, and Electron Attachment. *The Journal of Physical Chemistry A*, **119 (10)**, 2016–2025, doi:10.1021/jp5123344, URL http://dx.doi.org/10.1021/jp5123344.

US Environmental Protection Agency, 2016: Climate change indicators in the United States. EPA 430-R-16-004, URL https://www.epa.gov/climate-indicators.

von Clarmann, T., and Coauthors, 2003: Retrieval of temperature and tangent altitude pointing from limb emission spectra recorded from space by the Michelson Interferometer for Passive Atmospheric Sounding (MIPAS). *Journal of Geophysical Research: Atmospheres*, **108 (D23)**, n/a–n/a, doi:10.1029/2003JD003602, URL http://dx.doi.org/10.1029/2003JD003602, 4736.

von Clarmann, T., and Coauthors, 2009: Retrieval of temperature, H_2O, O_3, HNO_3, CH_4, N_2O, $ClONO_2$ and ClO from MIPAS reduced resolution nominal mode limb emission measurements. *Atmospheric Measurement Techniques*, **2 (1)**, 159–175, doi:10.5194/amt-2-159-2009, URL http://www.atmos-meas-tech.net/2/159/2009/.

Waugh, D., and T. M. Hall, 2002: Age of stratospheric air: Theory, observations, and models. *Reviews of Geophysics*, **40 (4)**, 1010, doi:10.1029/2000RG000101, URL http://doi.wiley.com/10.1029/2000RG000101.

List of Tables

Data source	Variables	Resolution	Time period	Reference
MIPAS	age from SF_6; temperature; pressure	zonal mean, 10° lat, 41 levels from 8 km to 54 km	2002–2012	Haenel et al. 2015
GOZ-CARDS	N_2O	zonal mean, 10° lat, 15 pressure levels from 100 to 0.46 hPa	2004–2014	Froidevaux et al. 2015, Andrews et al. 2001
EPA Climate Indicators	tropospheric N_2O	*in situ* surface	1980–2014	US EPA 2016
WACCM	SW; LW; temperature; ideal age; SF_6	2.5 ° lon, 1.875 ° lat, 31 pressure levels from 193 hPa to 0.3 hPa	1979–2014	Marsh et al., 2013, Garcia et al. 2017
JRA 55	SW; LW; temperature	1.25°×1.25°, 16 pressure levels from 225 hPa to 1 hPa	1979–2014	Kobayashi et al. 2015
MERRA	total dT/dt; temperature	1.25°×1.25°, 17 pressure levels from 200 hPa to 0.5 hPa	1979–2014	Rienecker et al. 2011
ERA-Interim	SW; LW; temperature	1°×1°, 26 pressure levels from 150 hPa to 0.5 hPa	1979–2014	Dee et al. 2011

Table 1. Data, reanalyses, and model output used in this study. SW is the shortwave radiation and LW is the longwave radiation.

List of Figures

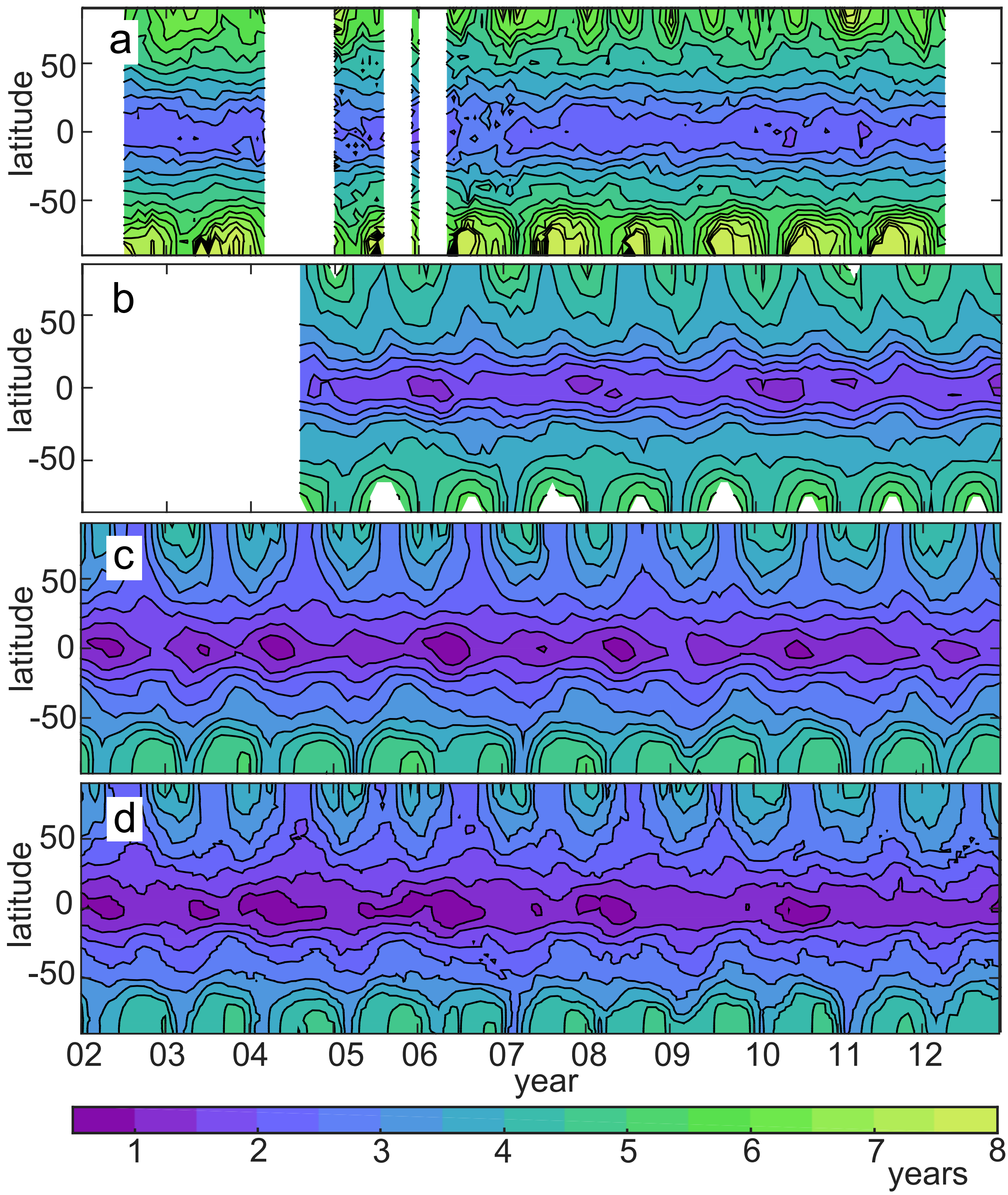

Figure 1. Age of air on the 500 K surface. (a) SF_6 from MIPAS, (b) N_2O from GOZCARDS, (c) SF_6 from WACCM, and (d) WACCM ideal age tracer. Contours are every half year, and the ages in the Southern Hemisphere winter for MIPAS get above 8 years old.

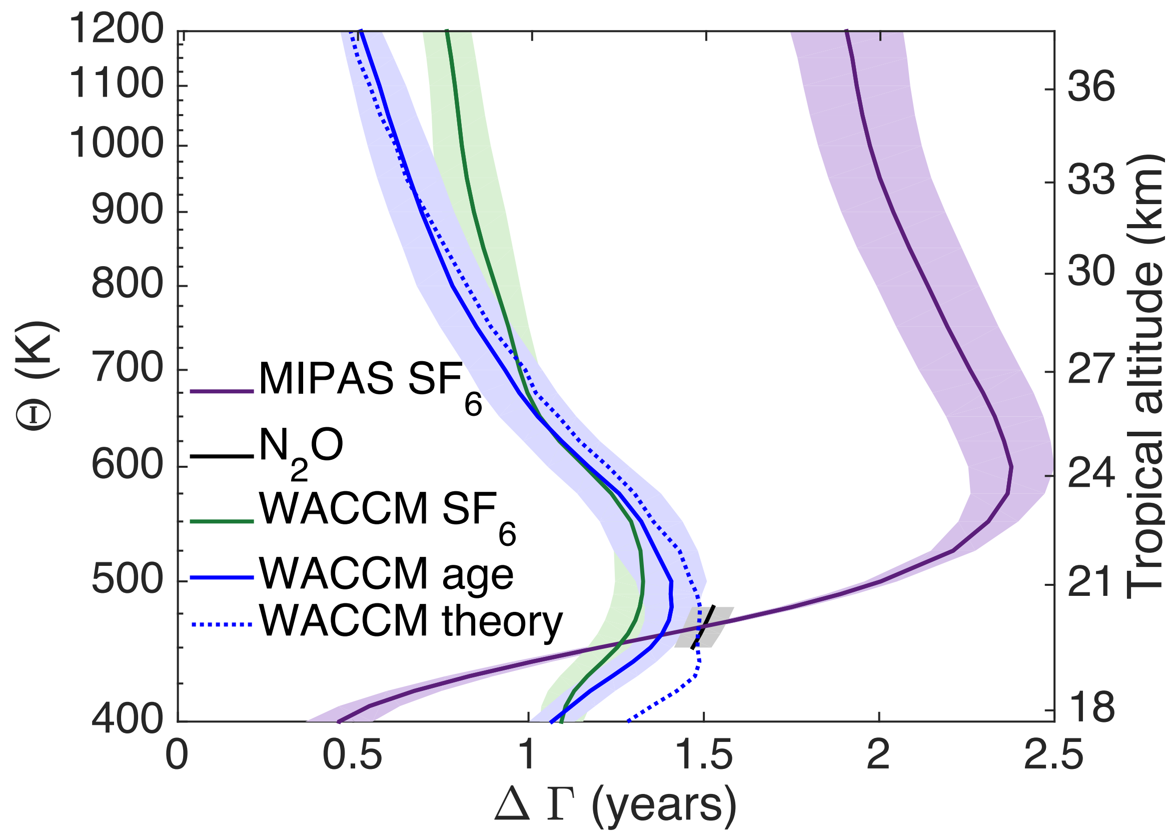

Figure 2. The average age difference between downwelling and upwelling age of air on each isentrope between 2007–2011. $\Delta\Gamma$ is plotted in solid lines: MIPAS SF_6-age in purple, GOZCARDS N_2O age in black, WACCM SF_6-age in green, and WACCM ideal age of air in the blue. The blue dotted line shows the ratio of the total mass above each isentrope to the mass flux through the isentrope ($M/\mathcal{M}$) from WACCM. The shading shows one standard deviation of the five annual averages that are averaged to get the mean. The mean height of each isentrope in the tropics (calculated from MIPAS pressure and temperature) is on the right y-axis.

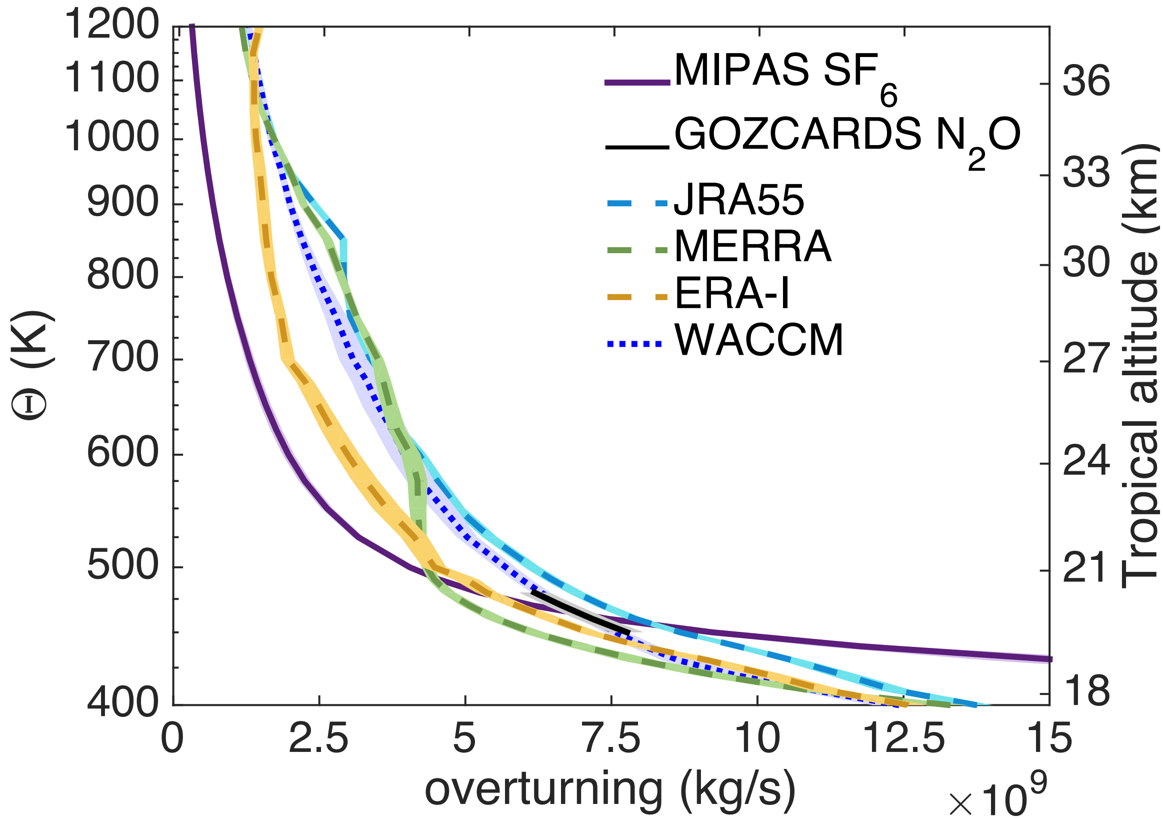

Figure 3. The strength of the total overturning circulation through each isentrope averaged between 2007–2011. The solid lines are for the data-based estimates MIPAS SF_6 is in purple and GOZCARDS N_2O in black. Reanalyses are shown in dashed lines: JRA 55 in light blue, MERRA in green and ERA-Interim in gold. The dotted blue line is WACCM. The shading shows one standard deviation of the five annual averages. The details of the calculation for each data product, the model, and the reanalyses are described in the text. The mean height of each isentrope in the tropics (calculated from MIPAS pressure and temperature) is on the right y-axis.